Light: Science & Applications (2017) 6, e17029; doi:10.1038/lsa.2017.29
Official journal of the CIOMP 2047-7538/17
www.nature.com/lsa

ORIGINAL ARTICLE

Nanoplasmonic mid-infrared biosensor for *in vitro* protein secondary structure detection

Dordaneh Etezadi[1], John B Warner IV[2,*], Francesco S Ruggeri[3,4,*], Giovanni Dietler[3], Hilal A Lashuel[2] and Hatice Altug[1]

Plasmonic nanoantennas offer new applications in mid-infrared (mid-IR) absorption spectroscopy with ultrasensitive detection of structural signatures of biomolecules, such as proteins, due to their strong resonant near-fields. The amide I fingerprint of a protein contains conformational information that is greatly important for understanding its function in health and disease. Here, we introduce a non-invasive, label-free mid-IR nanoantenna-array sensor for secondary structure identification of nanometer-thin protein layers in aqueous solution by resolving the content of plasmonically enhanced amide I signatures. We successfully detect random coil to cross β-sheet conformational changes associated with α-synuclein protein aggregation, a detrimental process in many neurodegenerative disorders. Notably, our experimental results demonstrate high conformational sensitivity by differentiating subtle secondary-structural variations in a native β-sheet protein monolayer from those of cross β-sheets, which are characteristic of pathological aggregates. Our nanoplasmonic biosensor is a highly promising and versatile tool for *in vitro* structural analysis of thin protein layers.
Light: Science & Applications (2017) **6,** e17029; doi:10.1038/lsa.2017.29; published online 25 August 2017

Keywords: label-free biosensing; nanoantennas; plasmonics; protein secondary structure; surface-enhanced infrared absorption spectroscopy

INTRODUCTION

Plasmonics has revitalized advanced label-free detection techniques by enabling extreme field confinement down to molecular dimensions, providing enhanced light-matter interaction at the nanoscale[1–4]. Engineering of plasmonic nanostructures has emerged as a powerful platform for biosensing through surface-enhanced detection in recent years, promoting new applications in molecular studies. In particular, surface-enhanced infrared absorption spectroscopy (SEIRA) with engineered plasmonic nanostructures has the unique ability to detect distinct IR vibrational signatures of a thin layer of molecules with normal incident far-field measurements[5–11]. The IR vibrational fingerprints provide atomic-level information on the molecular structures of biosamples such as lipids or proteins for detection, identification and diagnostic purposes[12–17]. Metallic nanoparticles, manufactured by top-down nanofabrication techniques, provide well-defined plasmonic resonances in the mid-infrared (mid-IR) range that can be tuned to target vibrational bands of molecules to access their rich spectroscopic information in a highly reproducible manner[18]. This property can enable them to serve as effective spectroscopic biosensors for detection and study of biological samples. Engineered mid-IR substrates with extremely high field enhancements at distinct frequencies enable the ultrasensitive IR detection of small amounts of biomolecules, including proteins[9,19,20]. The chemically specific SEIRA signals of protein amide band signatures extracted with plasmonic nanoantennas have been adopted for detection of protein monolayers and their interactions, due to their vital roles within living organisms[8,21]. Notably, the amide IR fingerprints resulting from protein-backbone vibrations provide comprehensive insight into the secondary-structural properties of proteins, and thus can provide information beyond basic detection limited to merely reporting their presence[22,23]. However, the unique properties of plasmonic biosensors consisting of nanoparticles tuned to molecular vibrational excitations have not been exploited to obtain secondary structure characteristics of protein monolayers in aqueous conditions. So far, the applications of mid-IR nanoplasmonics have been mainly focused on detecting the presence and orientations of molecules dried on the sensor surface, which is an undesirable environment for reliable protein conformational analysis[9,19–21,24].

Determination of secondary structures of proteins, which are governed by intramolecular and intermolecular hydrogen bonding, is crucial due to their role in major incurable diseases such as type II diabetes, prion and neurodegenerative disorders, including Huntington's (HD), Alzheimer's (AD) and Parkinson's (PD) diseases[25,26]. For instance, structural changes and misfolding of disease-related

[1]Bionanophotonic Systems Laboratory, École Polytechnique Fédérale de Lausanne (EPFL), Lausanne CH-1015, Switzerland; [2]Laboratory of Molecular Neurobiology and Neuroproteomics, EPFL, Lausanne CH-1015, Switzerland; [3]Institute of Physics, Laboratory of the Physics of Living Matter, EPFL, Lausanne CH-1015, Switzerland and [4]Department of Chemistry, Lensfield road, University of Cambridge, Cambridge CB21EW, UK
*These authors contributed equally to this work.
Correspondence: H Altug, Email: hatice.altug@epfl.ch
Received 13 July 2016; revised 17 February 2017; accepted 23 February 2017; accepted article preview online 27 February 2017

proteins and formation of nanoscale toxic fibrillar aggregates are considered the primary causes of those neurodegenerative disorders. The molecular mechanisms inducing the changes in secondary structure of such unstable proteins, their progressive accumulation into amyloid deposits and the consequent detrimental impact on cells remain unknown. Current technologies for protein studies, including nuclear magnetic resonance[27], X-ray crystallography[28], atomic force microscopy (AFM)[29–31] and circular dichroism[32] to name a few, have varied capabilities in accessing different levels of conformational information from secondary to quaternary structure. However, many of these methods face challenges and limitations regarding required sample properties, real-time observations of secondary structure changes under physiological conditions and scalability for multiplexed rapid screening. Some of these techniques demand expensive infrastructure or have strict requirements for preparation of homogeneous samples in large quantities, which restricts investigations on proteins that are costly and difficult to produce, such as amyloids or minute amounts of samples isolated from human tissues or cells. Likewise, some of the conventional techniques are limited to bulk measurements or thick layers of proteins, which are not suitable for mimicking nanometer-thin biological interfaces. Hence, providing non-destructive label-free technologies for *in vitro* detection of structural information of protein monolayers in their native states and in aqueous solution is highly advantageous in order to introduce a versatile tool for further understanding of the fundamental principles underlying disease-related conformational changes in proteins.

In this work, we determine the secondary-structural characteristics of thin layers of proteins with a mid-IR plasmonic nanoantenna array sensor. Our nanoplasmonic biosensor enables detection of conformational states of proteins in aqueous solution in a label-free, non-invasive manner. To demonstrate the capabilities of our platform, we investigate protein monolayers with different secondary and quaternary structure conformations by analyzing their amide I vibrational signatures, which are sensitive to protein-backbone conformation. The amide I band is highly advantageous for non-destructive structural detection of proteins since various secondary structures, including α-helices and β-sheets, correspond to distinct components of this band with specific vibrational frequencies within its range[22,23,33]. Here, by leveraging the plasmonically enhanced amide I signature from mid-IR nanoantenna biosensors and resolving its spectral content with second-derivative analysis, we extract secondary-structural information of protein layers in aqueous solution. This technique can provide unique possibilities for structural and functional studies on disease-related proteins. As a model system, we probe α-synuclein (α-Syn), an intracellular presynaptic protein that can misfold and form cross β-sheet rich fibrillar amyloid aggregates, resulting in degeneration of neurons and formation of Lewy bodies (LBs) and Lewy neurites (LNs), the main hallmarks of PD[34]. The cross β-sheet structure of amyloids has unique physical characteristics that differ from the β-sheet structure in native proteins. Our biosensor enables reliable measurements in dry and aqueous conditions with successful detection of conformational variations in disordered (random structured) monomeric monolayer and cross β-sheet structured fibrillated α-Syn protein immobilized on nanoantennas. Furthermore, we show that the acquired secondary structure signals and the extracted frequency range for the structural components are highly reproducible and flexible with the tuning of antenna resonances within the amide I region of protein fingerprints. Finally, we extract the secondary structure information of a monolayer of another model protein, i.e., streptavidin, with predominantly native β-sheet conformation immobilized on the biosensor. Notably, we are able to distinguish between the native and amyloidogenic β-sheet signals of these different proteins by observing the presence of the β-sheet components at higher wavenumbers for the native protein compared to the fibrillated α-Syn sample with pathological cross β-sheets. These results demonstrate the conformational sensitivity of our method in extracting subtle secondary-structural information from thin protein layers. Our experiments highlight the effectiveness of engineered plasmonic substrates as a versatile platform to access the conformational information of proteins in a sensitive and reliable manner in aqueous environment and at the monolayer level. Such a plasmonic biosensor is highly promising for delivering fundamental knowledge on the changes in protein conformations and their relation with disease mechanisms.

MATERIALS AND METHODS

Our biosensor platform consists of multiple arrays of rod-shaped gold nanoantennas engineered on a CaF_2 substrate for plasmonic resonant excitations of their dipole mode in the mid-IR frequency range, and the same array layout has been replicated on several CaF_2 chips (see Supplementary Fig. S1 of Supplementary Information for a schematic substrate-layout example). The resonance tuning of the nanorod array is governed by designing the aspect ratio of the antennas and the array period to efficiently reflect the light to the far field and maximize its coupling to vibrational fingerprints for spectroscopic biosensing[8,11,19,35–37]. Here, the antenna width and height are kept at constant values of 200 and 100 nm, respectively, based on our optimized nanofabrication process. This allows us to design their length (L) and the period (P) in different arrays in order to reliably tune the resonance peak and linewidth to provide collective plasmonic excitation at the wavenumber region of interest for incident light polarized along their length. Under such circumstances, the resonance peak frequency can be tuned based on its linear dependence on the antenna length and the refractive index of the surrounding environment according to $\lambda_P = \left(\frac{2}{m}\right) n_{eff} L + C$, where m is the order of the plasmonic mode, n_{eff} is the effective refractive index and C a constant value. The array period can be designed to yield higher field enhancements and optimized quality factor of the resonances by minimizing the radiative damping of the plasmonic response through the coupling of the retarded dipolar fields scattered by the antennas[19,35]. The nanorod antennas can be systematically engineered to have mid-IR plasmonic resonances with bandwidths larger than the absorption bands of proteins (i.e., amide I) in a reliable and reproducible manner (see Supplementary Fig. S3). Furthermore, the required dimensions and design accuracy of mid-IR nanorods are suitable for employing a wide range of reliable conventional nanofabrication techniques, such as nano-stencils[38] or e-beam lithography. Here, cleaned CaF_2 substrates are spin coated with methyl methacrylate (MMA) and polymethyl methacrylate (PMMA) resist double layer followed by electron-beam exposure using Vistec EBPG5000 (Jena, Germany) at 100 KV. Multiple metal nanoantenna arrays of 100 μm × 100 μm size with various values of L and P are identically formed on multiple CaF_2 substrates through a lift-off process by evaporating a thin Cr adhesion layer and 100 nm of Au with a Leybold Optics LAB 600H (Uzwil, Switzerland) e-beam evaporator. E-beam lithography enables reliable and reproducible fabrication of nanorods. Our plasmonic substrates are also highly robust and can be reused by employing appropriate cleaning procedures. Each nanoantenna array is one sensing area that is separately measured. Figure 1a shows an SEM image of a typical antenna array utilized in this work. The fabricated chips are cleaned with O_2 plasma treatment prior to initial Fourier transform infrared (FTIR) measurements[39]. Each nanorod

doi:10.1038/lsa.2017.29

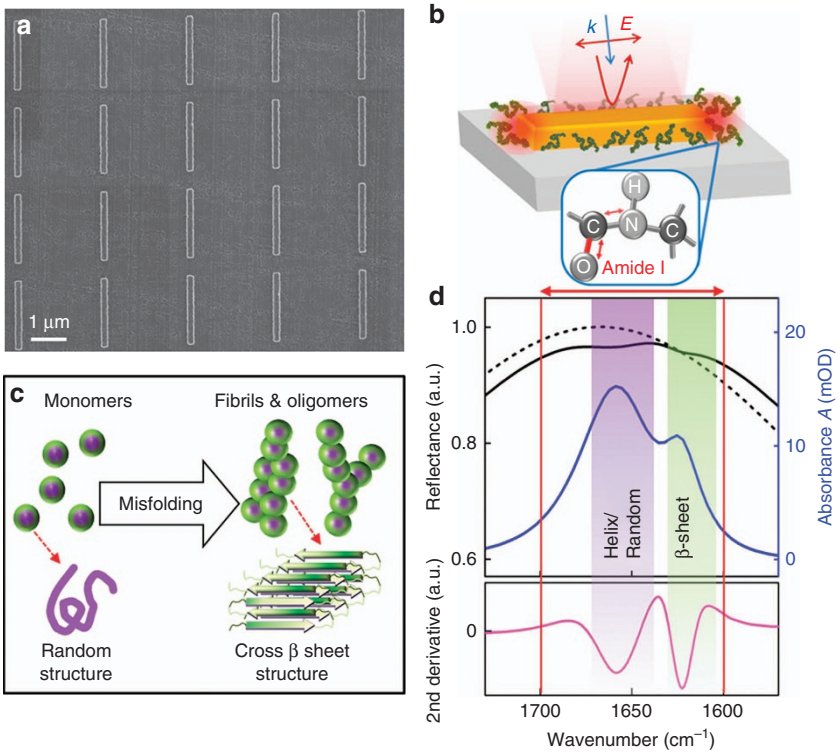

Figure 1 Plasmonic nanoantenna-array biosensor for spectroscopic detection of secondary structures of native and amyloidogenic proteins through characterization of amide I vibrational signatures by 2nd-derivative analysis. (**a**) SEM image of a typical Au nanorod antenna array with *L*: 2100 nm and *P*: 2.75 μm on CaF_2. (**b**) Schematic illustration of plasmonic resonance excitation in antennas tuned to the amide range by IR light polarized along the rod length. The inset depicts the amide I band of protein backbone vibration. The overlap of the plasmonic hot spots at the antenna tip ends with the proteins in the vicinity of the antennas results in enhanced absorption signals. (**c**) Illustration of the structural changes in the monomeric proteins from random structure to dominantly cross β-sheet aggregates through misfolding and amyloidogenic fibrillization. (**d**) Reflectance response of bare antenna arrays (dashed black) and antennas covered with a modeled thin layer (solid black). FDTD simulation is used for this depiction, in which a 5 nm layer of arbitrary complex refractive index (shown in Supplementary Fig. S2) is used to represent a typical protein layer on antennas. Blue curve shows the extracted absorbance signal from the simulated responses before and after covering with the modeled layer, with baseline correction. The bottom graph shows the 2nd derivative of the acquired signature, revealing the spectral components of amide I. The red arrow shows the amide I range in the mid-IR spectrum. The green area represents the approximate range for β-sheet components of secondary structure observable in fibrillated protein samples, whereas the purple area shows the approximate range for components of random structure or helices.

array is illuminated with IR light polarized along the length to provide resonance excitation and the reflected light is used to record the plasmonic response. A Bruker Vertex80V FTIR (Ettlingen, Germany) interferometer equipped with a Globar infrared source and KBr beamsplitter (4000-400 cm^{-1}), coupled to a Hyperion IR microscope with a linear polarizer, a Cassegrain objective (15 ×, NA = 0.4) and a liquid-nitrogen cooled mercury cadmium telluride (MCT) detector, is used for all IR measurements. The interferometer is maintained under vacuum while the microscope is purged with CO_2 and humidity-filtered air. Knife-edge apertures at the microscope are aligned with areas of the arrays (100 μm × 100 μm) for each measurement and a thick Au mirror is used for reference. Details of the data acquisition and analysis are reported in the Supplementary Information. As illustrated in Figure 1b and 1d, the interaction of the plasmonic field-enhanced antenna hot spots excited at the tip ends of rods with the protein in their vicinity provides SEIRA signals that are measured in the far field through the reflectance spectrum. A simulated response of an antenna array is used for illustration in Figure 1d, where the reflectance of bare antennas (without absorptive layer in their vicinity) designed for excitation in the amide I range is depicted as a dashed black curve. The reflectance with a thin (5 nm) modeled layer with a complex refractive index on antennas, representing a typical protein layer, is shown as a black solid line. The responses (*R*) of the array before and after covering with the thin layer are used to access the vibrational signatures of the layer, shown as blue curves, through extraction of the absorbance using the logarithmic ratio of the responses, $A = -\log(R_{with\ protein}/R_{bare})$[Ref. 8]. Finite-difference time-domain simulation was performed with commercial software of Lumerical FDTD Solutions. A plane-wave source with a linearly polarized electric field along the antenna length was defined for an array unit cell with $L = 2100$ nm and $P = 3$ μm. The dielectric values of the materials used were obtained from the Palik library for gold, along with a constant refractive index of $n = 1.4$ for CaF_2. A modeled complex refractive index was used as an arbitrary thin layer representing a typical protein (Supplementary Fig. S2).

We use our plasmonic biosensor to probe structural changes associated with the fibrillization of α-Syn. Monomeric α-Syn (WT) (from AnaSpec, Inc.), was diluted in 50 mM Tris HCl buffer with 150 mM NaCl at pH 7.5 and used in dry measurements. To induce fibrillization, a sample from the same stock was incubated on a shaker at 400 rpm at 37 °C for 10 days. For measurements of α-Syn in buffer solution, the Au surface of nanoantennas on each substrate was functionalized with COOH-functional alkane thiol self-assembled monolayer (SAM), MHDA (16-mercaptohexadecanoic acid, from Sigma-Aldrich), and synthesized amino-$(PEG)_2$-Maleimide linker. In these experiments, α-Syn monomeric samples with a C-terminal

sulfhydryl group (A140C) were utilized as described in Supplementary Information (Supplementary Figs. S5–S7). The monomeric stock of α-Syn A140C was prepared as mentioned before. Fibrillated protein samples for in-solution measurement were prepared with a mixture of 10% A140C and 90% WT α-Syn monomers (see Supplementary Information). For experiments with streptavidin (from Thermo Fisher Scientific), new plasmonic substrates were functionalized with biotinylated-PEG-alkane thiol ($C_{31}H_{58}N_4O_6S_2$, from Nanoscience Instruments). Details of all surface-functionalization steps for in-solution measurements are described in Supplementary Information.

RESULTS AND DISCUSSION

In our experiments, we analyzed the spectral features of the detected plasmonically enhanced signatures within the amide I range of the acquired data. Figure 1b illustrates the dry-condition measurements in which the antennas are illuminated from the top with linearly polarized incident light along their length. The schematic depiction shows the amide I signature of proteins, resulting mainly from the C = O stretching vibration of the peptide bonds ($\sim 80\%$) with a minor contribution from the C-N stretching vibration[23]. The overall secondary structure of the protein, which critically influences its functionality, represents the local folding of segments of its polypeptides into stable structures, including α-helices and β-sheets, or random coils (disordered). Depending on the secondary structure of the protein, the amide I band can include multiple absorption components with different frequencies within its range (1600–1700 cm^{-1}), as illustrated by an example in Figure 1d[22,23]. The amide I signals of proteins with turns, loops, random coils and helices (in general, non β-sheet strands) have components that are within 1645–1690 cm^{-1} with some overlaps among their ranges. However, the β-sheet structured samples have distinguishable components within the 1615–1640 cm^{-1} or 1680–1695 cm^{-1} ranges. The β-sheets in amyloidogenic proteins in fibrillar states are reported to appear at lower wavenumbers in the first range and at higher wavenumbers in the upper range, compared to native β-sheets[23]. To extract the conformational information of a protein, we apply second-derivative analysis of the amide I fingerprint to resolve its spectral content associated with the secondary structure[40]. The method of evaluating the second derivative of the amide I band has been used for protein spectroscopic studies as it provides a qualitative approach to detect the presence of different secondary structures by separating overlapping component bands of the acquired signals. As shown in the bottom graph in Figure 1d, by determining the frequency positions of the conformational components of the extracted amide I signal through this analysis, we can assess different secondary structure conformations in a sample protein, such as random coils or β-sheets. Here, the arbitrary thin layer is modeled with 2 Lorentzians in amide I range for illustration purposes to represent different structural components of a typical protein. The schematic illustration in Figure 1c represents the distinct conformational changes associated with the misfolding and fibrillization of α-Syn, a process that is central to the pathogenesis of neurodegenerative diseases, including PD and dementia[34]. α-Syn is an intrinsically random structured (disordered) protein and exists as monomers with disordered conformations in solution but can adopt α-helical conformations, for instance, upon membrane binding, or β-sheet structure when it forms amyloid-like fibrillar aggregates, which can be replicated *in vitro*[41,42]. As schematically represented in Figure 1d, the native random structured monomers and dominantly cross β-sheet structured fibrils of the pathological conformation of α-Syn give rise to spectrally different absorption components within the amide I band that can be extracted with the plasmonic substrate from a thin layer of proteins.

Protein secondary structure detection with plasmonic nanoantennas through amide I signature

We initially measured the amide I signal of α-Syn monomers and fibrils from a dried thin film formed by physisorption on gold antenna arrays to validate the extent of the obtained information using our system. For monomeric protein, each plasmonic substrate with multiple arrays was covered with 80 µl of protein solution at 12 µM concentration for an hour, followed by successive rinsing steps with Tris buffer and purified DI water for 10 min to remove excessive unbound proteins from the substrate. The reflectance response of one of the clean (bare) antenna arrays on a CaF_2 substrate (Chip 1) is shown in Figure 2a in black for antennas of length $L = 2200$ nm with array period $P = 2.85$ µm. The black curve in Figure 2b shows the response of the same array after physisorption of the α-Syn monomers and subsequent rinsing. The effects of absorption bands of amide I and amide II from the protein layer can be clearly observed in the reflectance response. The resulting absorbance signal for the monomeric α-Syn in Figure 2c (black) shows the acquired amide I and II bands. Successively, to extract the fibril signatures, we induced *in vitro* aggregation in α-Syn protein stock, as explained in the Materials and Methods section, and similarly acquired the protein spectra using a sample solution containing predominately amyloid fibrillar species of α-Syn with rich β-sheet conformation. For this structural state of protein, another plasmonic substrate (Chip 2) with multiple antenna arrays, including the same array design with $L = 2200$ nm and $P = 2.85$ µm, is used, for which the bare response is presented in Figure 2a in red. The two arrays used on these substrates have identical antenna design and bare reflectance to demonstrate the reproducibility of the fabrication and ensure that no variation from the plasmonic response of antennas could impact the resulting signals from the protein in the two states. Red curves in Figure 2b and 2c, show the response after physisorption of the fibrillated sample of α-Syn protein and the obtained absorbance from this array, respectively. The variation in the amide I peak of the α-Syn in the two measurements can be observed in Figure 2c. To analyze the content of protein secondary structure in these measurements, we applied second-derivative analysis on the extracted signals (A) within the amide I range and resolved the components corresponding to each structural conformation[40]. This analysis requires good signal-to-noise ratio of the acquired data, which our plasmonic sensor provides in the amide I region with the tailored resonances optimized for this vibrational band. Figure 2d shows the second-derivative of the resulting logarithmic reflectance ratio (A) for the α-Syn protein in the monomeric (black) and fibrillated (red) states. The results clearly demonstrate the difference between the two conformational states of α-Syn, as expected[43]. The monomeric sample, which exists predominantly in disordered conformation with slight α-helical propensity, has components only at wavenumbers above 1645 cm^{-1}. In the case of the fibrillated α-Syn samples, the presence of β-sheet structure is observed due to the existence of a component at the lower wavenumbers within the 1615–1640 cm^{-1} range in the red curve of Figure 2d. These results agree with previously reported measurements for fibrillated α-Syn samples in which the contributions of non-β-sheet components, such as loops, turns or disordered/random coils, are observed in addition to those of β-sheets[42,44,45] as the sample contains mixtures of fibrils and non-fibrillated proteins. Our AFM investigations on the plasmonic substrates indicate that physisorption of fibrillated α-Syn does not result in the formation of complete uniform monolayers on the sensor

doi:10.1038/lsa.2017.29

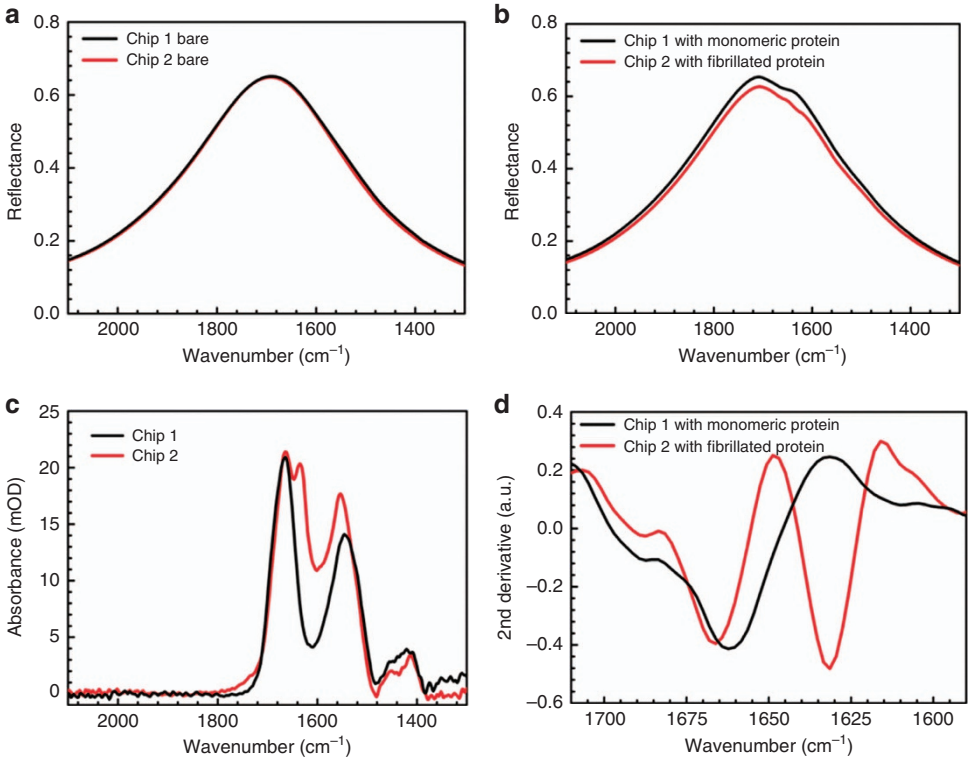

Figure 2 Spectroscopic detection of secondary structure components of monomeric and fibrillated α-Syn protein on plasmonic biosensors. (**a**) Bare reflectance response of clean antenna arrays with *L*: 2200 nm and *P*: 2.85 μm on two different substrates: an array on Chip 1 in black used for the monomeric α-Syn experiment and an array on Chip 2 in red used for the fibrillated α-Syn experiment. (**b**) Responses of the same antenna arrays shown in (a) after physisorption of monomeric α-Syn on Chip 1 (black) and fibrillated α-Syn on Chip 2 (red), followed by rinsing. (**c**) Extracted absorbance signals for monomeric (black) and fibrillated (red) α-Syn protein with baseline correction. (**d**) Second derivatives of the acquired logarithmic reflectance ratios (*A*) from monomeric (black) and fibrillated (red) α-Syn, showing the distinguished β-sheet signal in the aggregated samples.

surface, mainly due to the insoluble properties of fibrillar aggregates of the protein. Example images of this observation are presented in Supplementary Fig. S4, where uniform coverage can be observed on one of the arrays on Chip 1 with monomeric α-Syn, whereas aggregates of α-Syn fibrils are spotted at random locations on arrays of Chip 2. In addition, the surface roughness of the substrates and the fabricated nanorods, shown in Supplementary Fig. S4a, is a limiting factor for detailed investigation of the monomers or the fibrillated proteins with the AFM technique, for which atomically flat substrates are required to observe monomers or small oligomeric species[30,46]. While AFM was not able to easily resolve the monomers or fibrils on all the nanoplasmonic sensors, acquired protein signals from all antenna arrays on multiple chips manufactured under the same fabrication conditions successfully replicated and demonstrated the presence of monomers and fibrillated α-Syn proteins and their distinct characteristic secondary structure components in all experiments (example data are shown in Supplementary Figs. S3 and S11).

Random structured and amyloidogenic β-sheet protein-conformation detection with plasmonic substrates

Next, we tested the capabilities of our plasmonic nanoantenna platform to identify the secondary structure content of proteins in aqueous conditions. The overlap of the bending vibration of liquid water molecules with the amide I band of proteins limits highly sensitive mid-IR spectroscopic measurements in conventional IR transmission spectroscopy[47]. We previously demonstrated that our nanoplasmonic substrate, implemented in plasmonic internal-reflectance configuration, can overcome this limitation in normal incident microscopic measurements and enable mid-IR spectroscopic detection for a monolayer of proteins, even in the presence of water[8]. In this scheme, shown in Figure 3a, the reflectance responses of the arrays are collected through the back side of the IR-transparent CaF_2 substrate. The excited plasmonic resonance of the antennas provides field enhancements that decay exponentially away from the tip ends of the nanorods into the surrounding background, which results in extreme sensitivity to the antenna vicinity for biological assays. While the proteins are immobilized on the antenna by full coverage of the entire gold surface, the confinement of the plasmonic hot spots at the nanoantenna tip ends enables selective local probing at the tips, and therefore minimizing the interference from the water solution, which is ideal for spectroscopic measurements on thin protein monolayers in an aqueous environment[8]. Due to the increase in the refractive index of the environment in the vicinities of antennas in buffer, the antenna length and the array period are redesigned based on the linear dependence of the resonance on the effective refractive index of their surrounding environment. This allows us to match their plasmonic resonance to the amide I vibrational signature by decreasing the antenna length[8]. Here, the Au nanoantennas are functionalized with an SAM, which is a well-known and widely used method to covalently immobilize proteins. This technique, depicted in Figure 3a and Supplementary Fig. S5, is known for stable and reproducible monolayer formation on gold biosensors[48]. The functionalization procedure,

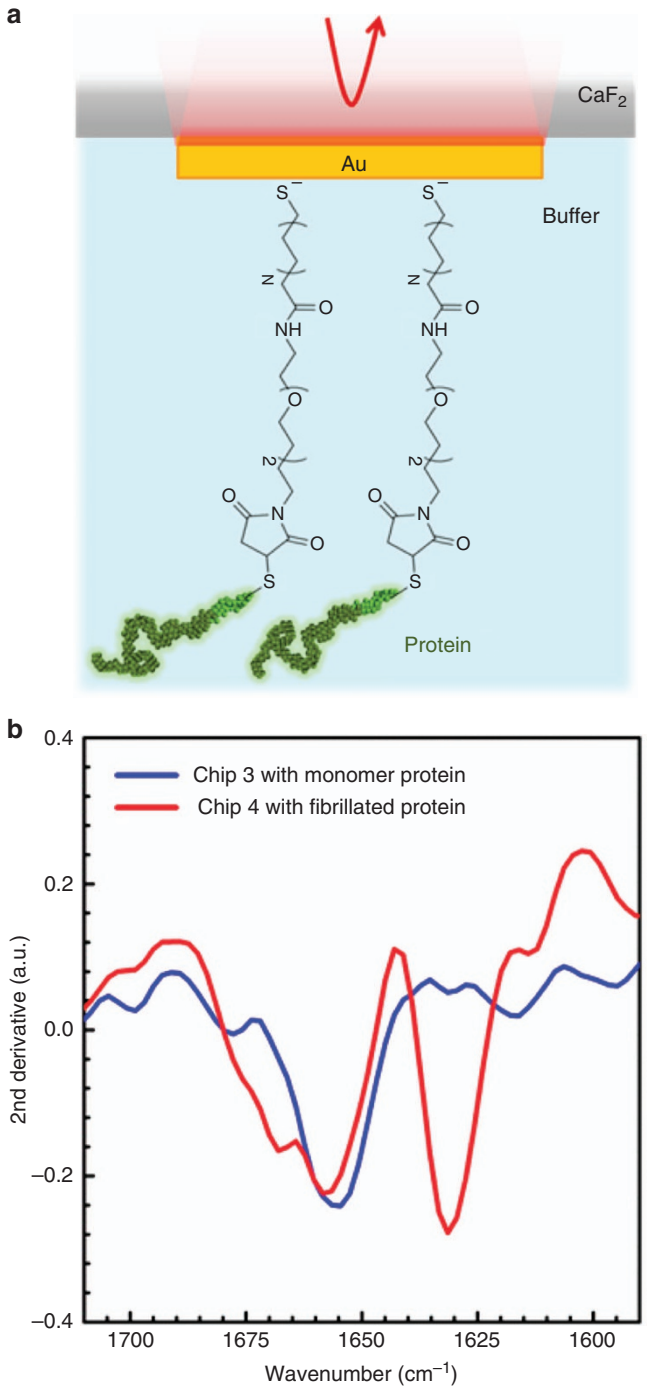

Figure 3 Spectroscopic detection of secondary structure components of monomeric and fibrillated α-Syn protein immobilized on plasmonic biosensors with SAM in buffer solution. (**a**) Schematic illustration of the in-solution measurement configuration from the backside of the CaF_2 substrate (not to scale), and the protein immobilization with MHDA/amino-$(PEG)_2$-maleimide linker. (**b**) Second derivatives of the acquired amide I signals measured in Tris buffer from monomeric (blue) and fibrillated (red) α-Syn, immobilized on Chips 3 and 4, respectively (similar antenna designs with *L*: 1850 nm and *P*: 2.6 μm), showing the distinguished β-sheet signal in the aggregated samples compared to random structured monomers.

described in Supplementary Information, involves attachment of an amino-$(PEG)_2$-maleimide linker through activation with sulfo-NHS/EDC chemistry (see Supplementary Information and Supplementary Figs. S5–S7 and S9 for details)[49]. The α-Syn protein, prepared with a terminal cysteine residue at its C-terminus to provide a sulfhydryl group for binding, was then immobilized on the nanoantennas through a thiol-maleimide Michael addition reaction with the maleimide linker[50]. This selective immobilization ensures the formation of a monolayer of protein samples with a stable covalent bond without introducing any detected additional absorption bands in the amide I region (shown in Supplementary Fig. S9). The reflectance responses of one of the antenna arrays ($L = 1850$ nm and $P = 2.6$ μm) on a plasmonic substrate with the alkane thiol SAM and after the immobilization of monomeric α-Syn with linker, are measured in aqueous environment (i.e., Tris buffer) and shown in Supplementary Fig. S8a (Chip 3). Next, another plasmonic substrate (Chip 4) with the same layout of multiple arrays including an identical antenna array ($L = 1850$ nm and $P = 2.6$ μm) was measured before and after immobilization of fibrillated α-Syn with the same procedure as described above; the reflectance responses for this array are shown in Supplementary Fig. S8b. To extract the conformational information of these protein layers measured in buffer, the second derivative of the logarithmic ratio of the reflectance responses before and after protein immobilization (A) was calculated as shown in Figure 3b, where the blue and red curves show the secondary structure components of the α-Syn for the two cases before and after inducing fibrillization in the protein sample, respectively. As expected, the blue curve of the monomeric α-Syn protein indicates the presence of secondary structure components, above 1645 cm^{-1}, representing disordered (random) conformations without distinct β-sheet content. However, a distinguished β-sheet structure is detected in the red curve representing the structural content and conformation in the cross-β state of fibrillated α-Syn. While the water absorption can be observed in the reflectance response of the antenna arrays measured in buffer (Supplementary Fig. S8 and Figure 4a), the acquired signals at the amide I range with plasmonic substrate enable reliable spectroscopic measurements. These results indicate that our biosensor can successfully resolve the two distinct secondary structure components for the β-sheet and the non-β-sheet strands (random, turns or loops) in a thin layer of protein samples measured in buffer solution in a reliable and reproducible manner (see Supplementary Fig. S12 for more replications of the data).

Effect of resonance-excitation conditions on acquired protein structural information

The signal enhancements achieved with our plasmonic nanoantennas for detection of protein absorption signatures depend on the spectral matching of their resonances with the vibrational bands of the biomolecules[19]. In this regard, it is important to determine the sensitivity of the acquired amide I components to the resonance-tuning conditions for reliable detection of conformational information. We experimentally investigated the detected structural components of the proteins acquired from arrays with peak resonances throughout and beyond the amide I region in aqueous solution. These results are shown in Figure 4a and 4b for secondary structure components of the fibrillated α-Syn extracted from arrays tuned in a wide wavenumber range and with varied linewidths of the resonances. Figure 4a shows the reflectance of the fabricated antenna arrays functionalized with alkane thiol SAM in the buffer solution before immobilization of protein, demonstrating a broad tuning range of the resonance peaks, as large as 200 cm^{-1}, and different resonance

doi:10.1038/lsa.2017.29

linewidths from 350 to 500 cm^{-1}. This resonance tuning is obtained by designing multiple arrays with antenna lengths ranging from 1850 to 2050 nm and array periods from 2.3 to 2.6 μm. Figure 4b shows the resulting components of the amide I through second-derivative analysis of the content of the acquired data for each antenna array after protein immobilization as described before. As shown here, all the extracted signals are similar to one another with minor variations, which indicates that the multiple components of the secondary structure can be reliably resolved with our biosensor despite slight variations of the plasmonic resonance-peak position within the amide I region. To further emphasize this property of our biosensor, we extracted the locations of structural components of the α-Syn sample from multiple antenna arrays tuned within the amide I range ($L = 1850$, 1900, 1950, 2000, 2050, 2100 nm and $P = 2.3$, 2.4, 2.5, 2.6 μm). Our experimental observations are summarized in Figure 4c, in which the acquired secondary structure components of monomeric and fibrillated α-Syn proteins in buffer from 21 arrays with different resonance conditions are shown. The graph represents the detected frequency of each component from the acquired protein amide I second-derivative data versus the resonance peak of the antenna array used in each corresponding measurement. To extract the resonance peak from each reflectance spectrum, a Lorentzian fit is used (see Supplementary Fig. S10). The circular data points in multiple colors represent the different components extracted from the measurements of the aggregated fibrillar α-Syn protein, for which three distinguished components could be observed in all of the measurements, demonstrating the presence of β-sheet and non-β-sheet (random, turns or loops) strands. The data points presented as blue triangles show that in the monomeric α-Syn sample, one component representing disordered (random) structure (with α-helical propensity) can be detected, even with variation in the resonance condition of the plasmonic biosensor. As observed here, despite a large tuning range of the resonances beyond the amide I range, the detected β-sheet component of the fibrillated protein sample exhibits only minor variations within 5 cm^{-1}, and the additional non-β-sheet components can be resolved successfully. Our results indicate that while optimized matching of our nanoantenna-array resonance peak to the vibrational amide bands provides maximum enhanced absorption signals for spectroscopic detection, the multiple components of the secondary-structural conformation can be reliably acquired through second-derivative analysis of the extracted amide I signals without strong dependence on the conditions of resonance matching and coupling with this vibrational band, even in the presence of water. These properties indicate the reliability of our biosensing platform of nanoantenna arrays, even in the potential case of minor manufacturing variations induced by any employed nanofabrication technique.

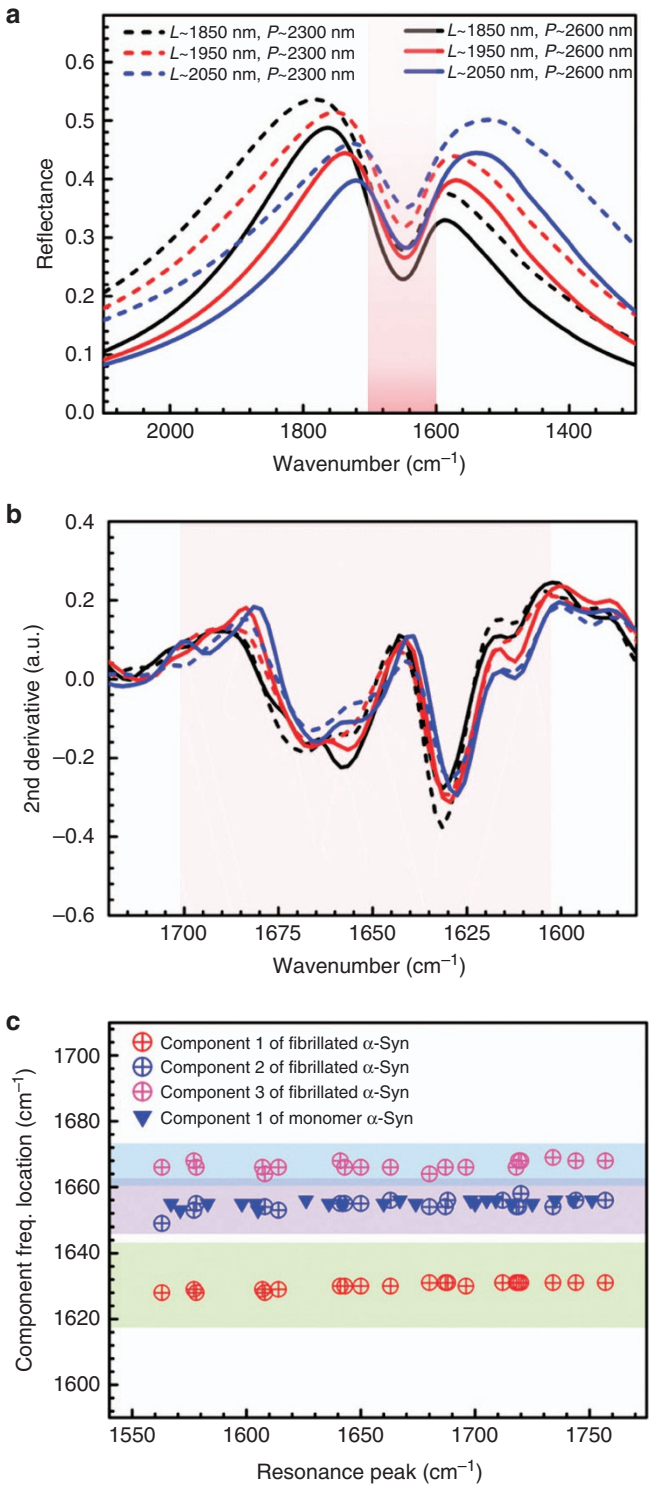

Figure 4 Tolerance of plasmonic-antenna resonance-peak matching within the amide I range for secondary structure detection. (**a**) Reflectance responses of antenna arrays with *L*: 1850 nm (black), 1950 nm (red) and 2050 nm (blue) with *P*: 2.3 μm (dashed) and 2.6 μm (solid) covered with SAM of MHDA, measured in Tris. The pink shaded area shows the amide I range. (**b**) The corresponding second-derivative data of the extracted amide I signals from the same arrays as in **a** after immobilization of fibrillated α-Syn. (**c**) Frequencies of the acquired secondary structure components within the amide I band versus the reflectance peaks of the antenna arrays with different resonance conditions for measurements in buffer solution. Circular data points are extracted components of the fibrillated α-Syn measurements, whereas the blue triangular data points are from the monomeric protein. The light-green shaded area shows the components corresponding to β-sheets, the purple area corresponds to random structures (or helices) and the blue area shows the additional components, including turns and loops.

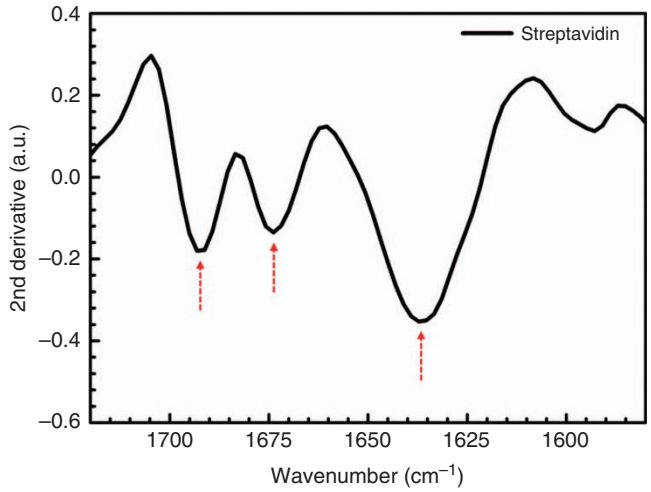

Figure 5 Secondary structure components of the amide I absorption band of streptavidin immobilized via biotin binding. The three minima correspond to native β-sheets (within 1615–1645 cm^{-1} and 1680–1695 cm^{-1}) and β turns (within 1665–1690 cm^{-1}) of secondary structures of the immobilized protein measured in phosphate buffer saline (PBS), on one array with *L*: 1900 nm and *P*: 2.5 μm.

Distinguishing native from pathological β-sheet protein conformations

Conformational studies of proteins require sensitive detection of structural content in order to enable their evaluation and extract subtle differences in their secondary structure. For instance, β-sheet conformations exhibit variations in different proteins that reflect their functional diversity in health and diseases. Therefore, it is important for a detection technique to sensitively access and distinguish detailed structural information of proteins in order to elucidate their characteristics. To evaluate this capability, we employed our platform to extract the secondary-structural information of another protein monolayer, streptavidin (SA), with a rich native β-sheet conformation[51]. The SA protein is immobilized on our nanoantenna biosensor through its high binding affinity to biotin. First, the plasmonic substrate is functionalized by incubation in a solution of biotinylated-PEG-alkane thiol (BAT), followed by rinsing, before initial measurement in phosphate buffer saline (PBS). Next, SA protein solution at 50 μg /ml in PBS was immobilized on all the arrays of the substrate, followed by rinsing with PBST (PBS with 0.05% Tween 20) and PBS to remove unbound proteins before measuring the arrays with protein monolayer in buffer. The second-derivative of the extracted amide I signatures from an array with $L = 1900$ nm and $P = 2.5$ μm in this experiment is shown in Figure 5. Here, the secondary structure components in the amide I range correspond to β-sheet structures observed within the 1635–1640 cm^{-1} and 1690–1695 cm^{-1} ranges, in addition to a component of β turns in the range of 1670–1675 cm^{-1} and some indications of a small presence of coils in this protein. Notably, the extracted signal detected in this native β-sheet protein is observed at slightly higher wavenumbers compared to the cross β-sheet component of the aggregated α-Syn protein (shown in Figure 3b and 4b). This result was consistently observed, even with intentional tuning of the nanoantenna design for resonances within the amide I range (data shown in Supplementary Fig. S14). This is in agreement with previous observations in which the redshift of this component is observed for fibrillar β-sheets within amyloid aggregates relative to native proteins[23,52,53]. These results demonstrate that our biosensor can enable the distinction between native and pathological β-sheet conformations and indicate that our technique has the capability to extract detailed structural information of protein monolayers for conformational investigations.

CONCLUSION

The effectiveness of the engineered plasmonic nanoantennas in producing signal enhancements to many orders of magnitude in specific mid-IR vibrational bands of interest has been employed in the detection of different biomolecules, including proteins and lipids. However, previous studies did not incorporate investigation of the spectral content within individual absorption bands of plasmonically detected functional groups. In particular, the amide I signatures of proteins consisting of multiple overlapping components contain important information on the protein secondary-structural properties. In this work, we have expanded the sensing capabilities of metallic mid-IR nanostructures to sensitively probe and differentiate the secondary-structural compositions in protein monolayers. Using second-derivative analysis of the accessed amide I vibrational signatures from thin layers of protein on nanoantennas in dry conditions, we resolved the secondary-structural components and confirmed the detection of a conformational change from random coil to cross β-sheet as a result of aggregation in α-Syn protein. Furthermore, we implemented our sensor in a plasmonic internal-reflectance scheme and successfully detected the conformational information of a monolayer of α-Syn protein in an aqueous environment. Based on our experimental results, we can distinguish the monomeric α-Syn protein from the fibrillated α-Syn sample, including multiple conformational components of β-sheets, turns and random structures. These results are confirmed to be tolerant to the tuning of the resonance peak and linewidth of nanoantennas within the amide I range. Moreover, we demonstrated the capability of our sensor to resolve variations of conformational details by distinguishing the secondary structure information of another protein with predominantly native β-sheet conformation from that of the aggregated cross β-sheet α-Syn. Our experiments with different protein secondary structures and immobilization conditions indicate that this plasmonic biosensor is a highly promising platform, applicable to sensitive detection and a broad range of investigations of protein conformational properties. It is also important to emphasize that the acquired secondary structure signals of monolayer proteins from each nanoantenna array correspond to minute amount of proteins immobilized on the antenna surface. For instance, for the case of α-Syn monomers, the extracted structural information presented in Figure 3b corresponds to a monolayer covering the gold surface of each antenna (i.e., $\sim 0.78\ \mu m^2$) in one array. Considering the size of an α-Syn monomer, with an approximate radius of gyration of 3 nm, and assuming full coverage of all the gold surfaces of the antennas, the presented result corresponds to α-Syn monomers estimated in the femtomole range measured in buffer. Our technique sensitively determines different secondary structure components of proteins in aqueous solution in a highly reproducible and reliable manner and offers the potential to observe minor secondary-structural changes induced in minute amounts of protein samples (see Supplementary Fig. S13), for instance, upon biomolecular interactions. Employing the unique features of engineered mid-IR nanophotonic substrates in plasmonic excitations, our chip-based sensor can enable new possibilities to deterministically tailor resonances to reveal the spectral content of detected absorption bands with high spectral resolution. For instance, the resonant characteristics of plasmonic substrates can be adapted to incorporate other important

doi:10.1038/lsa.2017.29

absorption bands besides amide I in proteins for in-depth analysis of structural properties and provide insight into higher-order conformational characteristics. This surface-sensitive nanoplasmonic biosensor can provide a robust and highly scalable tool for applications demanding rapid screening, such as drug discovery and pharmacology. In addition, the cost of our method could be largely scaled down by using inexpensive nanofabrication techniques to manufacture plasmonic nanorods. Furthermore, our nanoplasmonic sensor can be integrated with compact and low-cost on-chip FTIR spectrometers[54] or tunable mid-IR sources such as quantum cascade lasers, as well as advanced microfluidics, to exploit the rich information content of the mid-IR spectrum and have significant impact on numerous fields ranging from biochemistry to materials science.

CONFLICT OF INTEREST

The authors declare no conflict of interest.

ACKNOWLEDGEMENTS

We acknowledge École Polytechnique Fédérale de Lausanne (EPFL) and the Center of MicroNano Technology (CMi) for financial support and nanofabrication. This work was also partially supported by the European Research Council (ERC) under the European Union's Horizon 2020 research and innovation programme (Grant No. 682167), European Commission Horizon 2020 (grant no. FETOPEN-737071) and Swiss National Foundation for Science (Grant No. 152958, SNF31003A_146680, P2ELP2_162116 and P300P2_171219).

1 Arroyo OJ, Kukura P. Non-fluorescent schemes for single-molecule detection, imaging and spectroscopy. *Nat Photonics* 2016; **10**: 11–17.
2 Stockman MI. Nanoplasmonic sensing and detection. *Science* 2015; **348**: 287–288.
3 Brolo AG. Plasmonics for future biosensors. *Nat Photonics* 2012; **6**: 709–713.
4 Stanley R. Plasmonics in the mid-infrared. *Nat Photonics* 2012; **6**: 409–411.
5 Brown LV, Yang X, Zhao K, Zheng BY, Norlander P *et al.* Fan-shaped gold nanoantennas above reflective substrates for surface-enhanced infrared absorption (SEIRA). *Nano Lett* 2015; **15**: 1272–1280.
6 Rodrigo D, Limaj O, Janner D, Etezadi D, Garcia de Abajo FJ *et al.* Mid-infrared plasmonic biosensing with graphene. *Science* 2015; **349**: 165–168.
7 Srajer J, Schwaighofer A, Ramer G, Rotter S, Guenay B *et al.* Double-layered nanoparticle stacks for surface enhanced infrared absorption spectroscopy. *Nanoscale* 2014; **6**: 127–131.
8 Adato R, Altug H. *In-situ* ultra-sensitive infrared absorption spectroscopy of biomolecule interactions in real time with plasmonic nanoantennas. *Nat Commun* 2013; **4**: 2154.
9 De Ninno A, Ciasca G, Gerardino A, Calandrini E, Papi M *et al.* An integrated superhydrophobic-plasmonic biosensor for mid-infrared protein detection at the femtomole level. *Phys Chem Chem Phys* 2015; **17**: 21337–21342.
10 Pryce IM, Kelaita YA, Aydin K, Atwater HA. Compliant metamaterials for resonantly enhanced Infrared absorption Spectroscopy and refractive index sensing. *ACS Nano* 2011; **5**: 8167–8174.
11 Neubrech F, Pucci A, Cornelius TW, Karim S, García-Etxarri A *et al.* Resonant plasmonic and vibrational coupling in a tailored nanoantenna for Infrared detection. *Phys Rev Lett* 2008; **101**: 157403.
12 Ataka K, Kottke T, Heberle J. Thinner, smaller, faster: IR techniques to probe the functionality of biological and biomimetic systems. *Angew Chem Int Ed* 2010; **49**: 5416–5424.
13 López-Lorente ÁI, Mizaikoff B. Mid-infrared spectroscopy for protein analysis: potential and challenges. *Anal Bioanal Chem* 2016; **408**: 2875–2889.
14 Kwak JT, Kajdacsy-Balla A, Macias V, Walsh M, Sinha S *et al.* Improving prediction of prostate cancer recurrence using chemical imaging. *Sci Rep* 2015; **5**: 8758.
15 Berweger S, Nguyen DM, Muller EA, Bechtel HA, Perkins TT *et al.* Nano-chemical infrared imaging of membrane proteins in lipid bilayers. *J Am Chem Soc* 2013; **135**: 18292–18295.
16 Roy S, Covert PA, FitzGerald WR, Hore DK. Biomolecular structure at solid-liquid interfaces as revealed by nonlinear optical spectroscopy. *Chem Rev* 2014; **114**: 8388–8415.
17 Peng CS, Baiz CR, Tokmakoff A. Direct observation of ground-state lactam-lactim tautomerization using temperature-jump transient 2D IR spectroscopy. *Proc Natl Acad Sci U S A* 2013; **110**: 9243–9248.
18 Dregely D, Neubrech F, Duan HG, Vogelgesang R, Giessen H. Vibrational near-field mapping of planar and buried three-dimensional plasmonic nanostructures. *Nat Commun* 2013; **4**: 2237.
19 Adato R, Yanik AA, Amsden JJ, Kaplan DL, Omenetto FG *et al.* Ultra-sensitive vibrational spectroscopy of protein monolayers with plasmonic nanoantenna arrays. *Proc Natl Acad Sci U S A* 2009; **106**: 19227–19232.
20 Cetin AE, Etezadi D, Altug H. Accessible nearfields by nanoantennas on nanopedestals for ultrasensitive vibrational spectroscopy. *Adv Opt Mater* 2014; **2**: 866–872.
21 Wu CH, Khanikaev AB, Adato R, Arju N, Yanik AA *et al.* Fano-resonant asymmetric metamaterials for ultrasensitive spectroscopy and identification of molecular monolayers. *Nat Mater* 2011; **11**: 69–75.
22 Barth A. Infrared spectroscopy of proteins. *Biochim Biophys Acta* 2007; **1767**: 1073–1101.
23 Fabian H, Naumann D. *Protein Folding and Misfolding: Shining Light by Infrared Spectroscopy.* Heidelberg: Springer; 2012.
24 Alici KB, Gallardo IF. Detecting secondary structure and surface orientation of helical peptide monolayers from resonant hybridization signals. *Sci Rep* 2013; **3**: 2956.
25 Knowles TPJ, Vendruscolo M, Dobson CM. The amyloid state and its association with protein misfolding diseases. *Nat Rev Mol Cell Biol* 2014; **15**: 384–396.
26 Irwin DJ, Lee VMY, Trojanowski JQ. Parkinson's disease dementia: convergence of α-synuclein, tau and amyloid-β pathologies. *Nat Rev Neurosci* 2013; **14**: 626–636.
27 Wuthrich K. Protein structure determination in solution by nuclear magnetic resonance spectroscopy. *Science* 1989; **243**: 45–50.
28 Boutet S, Lomb L, Williams GJ, Barends TR, Aquila A *et al.* High-resolution protein structure determination by serial femtosecond crystallography. *Science* 2012; **337**: 362–364.
29 Adamcik J, Jung JM, Flakowski J, De Los Rios P, Dietler G *et al.* Understanding amyloid aggregation by statistical analysis of atomic force microscopy images. *Nat Nanotechnol* 2010; **5**: 423–428.
30 Ruggeri FS, Adamcik J, Jeong JS, Lashuel HA, Mezzenga R *et al.* Influence of the β-Sheet content on the mechanical properties of aggregates during amyloid fibrillization. *Angew Chem* 2015; **54**: 2462–2466.
31 Amenabar I, Poly S, Nuansing W, Hubrich EH, Govyadinov AA *et al.* Structural analysis and mapping of individual protein complexes by infrared nanospectroscopy. *Nat Commun* 2013; **4**: 2890.
32 Greenfield NJ. Using circular dichroism spectra to estimate protein secondary structure. *Nat Protoc* 2006; **1**: 2876–2890.
33 Kong J, Yu S. Fourier transform infrared spectroscopic analysis of protein secondary structures. *Acta Biochim Biophys Sin (Shanghai)* 2007; **39**: 549–559.
34 Lashuel HA, Overk CR, Oueslati A, Masliah E. The many faces of α-synuclein: from structure and toxicity to therapeutic target. *Nat Rev Neurosci* 2013; **14**: 38–48.
35 Adato R, Yanik AA, Wu CH, Shvets G, Altug H. Radiative engineering of plasmon lifetimes in embedded nanoantenna arrays. *Opt Express* 2010; **18**: 4526–4537.
36 Maß TWW, Taubner T. Incident angle-tuning of infrared antenna array resonances for molecular sensing. *ACS Photonics* 2015; **2**: 1498–1504.
37 Selig O, Siffels R, Rezus YLA. Ultrasensitive ultrafast vibrational spectroscopy employing the near field of gold nanoantennas. *Phys Rev Lett* 2015; **114**: 233004.
38 Aksu S, Yanik AA, Adato R, Artar A, Huang M *et al.* High-throughput nanofabrication of infrared plasmonic nanoantenna arrays for vibrational nanospectroscopy. *Nano Lett* 2010; **10**: 2511–2518.
39 Griffiths PR, de Haseth JA. *Fourier Transform Infrared Spectrometry.* 2nd edn. Hoboken: John Wiley & Sons; 2007.
40 Dong AC, Huang P, Caughey WS. Protein secondary structures in water from second-derivative amide I infrared spectra. *Biochemistry* 1990; **29**: 3303–3308.
41 Ramakrishnan M, Jensen PH, Marsh D. Association of α-synuclein and mutants with lipid membranes: spin-label ESR and polarized IR. *Biochemistry* 2006; **45**: 3386–3395.
42 Lee D, Park CW, Paik SR, Choi KY. The modification of α-synuclein by dicarbonyl compounds inhibits its fibril-forming process. *Biochim Biophys Acta* 2009; **1794**: 421–430.
43 Kulik AJ, Ruggeri FS, Gruszecki WI, Dietler G. Nanoscale infrared spectroscopy of light harvesting proteins, amyloid structures and collagen fibres. *Microsc Anal* 2014; **28**: 11–15.
44 Munishkina L, Phelan C, Uversky VN, Fink AL. Conformational behavior and aggregation of α-synuclein in organic solvents: modeling the effects of membranes. *Biochemistry* 2003; **42**: 2720–2730.
45 Bousset L, Pieri L, Ruiz-Arlandis G, Gath J, Jensen PH *et al.* Structural and functional characterization of two alpha-synuclein strains. *Nat Commun* 2013; **4**: 2575.
46 Khalaf O, Fauvet B, Oueslati A, Dikiy I, Mahul-Mellier AL *et al.* The H50Q mutation enhances α-synuclein aggregation, secretion, and toxicity. *J Biol Chem* 2014; **289**: 21856–21876.
47 Yang H, Yang S, Kong J, Dong A, Yu S. Obtaining information about protein secondary structures in aqueous solution using Fourier transform IR spectroscopy. *Nat Protoc* 2015; **10**: 382–396.
48 Love JC, Estroff LA, Kriebel JK, Nuzzo RG, Whitesides GM. Self-assembled monolayers of thiolates on metals as a form of nanotechnology. *Chem Rev* 2005; **105**: 1103–1170.
49 Zimmermann JL, Nicolaus T, Neuert G, Blank K. Thiol-based, site-specific and covalent immobilization of biomolecules for single-molecule experiments. *Nat Protoc* 2010; **5**: 975–985.
50 Nair DP, Podgórski M, Chatani S, Gong T, Xi W *et al.* The thiol-Michael addition click reaction: a powerful and widely used tool in materials chemistry. *Chem Mater* 2014; **26**: 724–744.
51 González M, Bagatolli LA, Echabe I, Arrondo JLA, Argaraña CE *et al.* Interaction of biotin with streptavidin thermostability and conformational changes upon binding. *J Biol Chem* 1997; **272**: 11288–11294.

52 Zandomeneghi G, Krebs MRH, McCammon M, Fändrich M. FTIR reveals structural differences between native β-sheet proteins and amyloid fibrils. *Protein Sci* 2004; **13**: 3314–3321.
53 Shivu B, Seshadri S, Li J, Oberg KA, Uversky VN *et al.* Distinct β-Sheet structure in protein aggregates determined by ATR-FTIR spectroscopy. *Biochemistry* 2013; **52**: 5176–5183.
54 Khalil D, Sabry Y, Omran H, Medhat M, Hafez A *et al.* Characterization of MEMS-FTIR spectrometer. Proceedings of SPIE 7930, MOEMS and Miniaturized Systems X, 79300J. SPIE: San Francisco, CA, USA; 2011.

Supplementary Information for this article can be found on the *Light: Science & Applications*' website (http://www.nature.com/lsa).